JOURNAL OF GEOPHYSICAL RESEARCH, VOL. 97, NO. A10, PAGES 14,967–14,976, OCTOBER 1, 1992

Funnel-Shaped, Low-Frequency Equatorial Waves

S. A. BOARDSEN,[1,2] D. L. GALLAGHER,[1] D. A. GURNETT,[3]
W. K. PETERSON,[4] AND J. L. GREEN[5]

Funnel-shaped, low-frequency radiation, as observed in frequency time spectrograms, are frequently found at the Earth's magnetic equator. At the equator the radiation often extends from the proton cyclotron frequency up to the lower hybrid frequency. Ray-tracing calculations can qualitatively reproduce the observed frequency-time characteristics of these emissions if the waves are propagating in the fast magnetosonic mode starting with wave normal angles of ~88° at the magnetic equator. The funnel-shaped emissions are consistent with generation by protons with a ring-type velocity space distribution. A ring-shaped region of positive slope in the velocity space density distribution of protons is observed near the Alfvén velocity, indicating that the ring protons strongly interact with the waves. Ray-tracing calculations show that for similar equatorial wave normal angles lower-frequency fast magnetosonic waves are more closely confined to the magnetic equator than higher-frequency fast magnetosonic waves. For waves refracted back toward the equator at similar magnetic latitudes, the lower-frequency waves experience stronger damping in the vicinity of the equator than higher-frequency waves. Also, wave growth is restricted to higher frequencies at larger magnetic latitudes. Wave damping at the equator and wave growth off the equator favors equatorial wave normal angle distributions which lead to the funnel-shaped frequency time characteristic.

1. INTRODUCTION

Low-frequency electromagnetic emissions between the proton cyclotron frequency and lower hybrid frequency are frequently observed near the Earth's magnetic equator [*Russell et al.*, 1970; *Gurnett*, 1976]. These waves are believed to play an important role in transferring energy from energetic protons convecting Earthward from the plasma sheet, to ionospheric thermal ions flowing along the magnetic field lines. Heating of the thermal ions (~1 — 10 eV) by these waves [*Curtis*, 1985] could explain the high correlation that has been observed between the occurrence of these waves and the occurrence of trapped equatorial ions (~50 — 100 eV) near the outer edge of the plasmapause [*Olsen*, 1987]. The frequency-time characteristic of the equatorial emissions shows a variety of forms. Often the waves are observed to have a funnel-shaped appearance on a frequency-time spectrogram, particularly when the spacecraft passes latitudinally through the magnetic equator. The purpose of this paper is to propose an explanation for the funnel-shaped structure of these emissions. The observational data will be discussed in section 2, and our interpretation of the funnel will be given in section 3, followed by a discussion.

2. OBSERVATIONS

An example of a funnel-shaped equatorial plasma wave is shown in Figure 1. This plot is a frequency-time spectrogram of the electric field spectral density measured by the sweep frequency receiver (SFR) on the Dynamics Explorer 1 (DE 1) spacecraft [*Shawhan et al.*, 1981]. The SFR samples the electric field intensity detected by a 215-m electric dipole antenna and the magnetic field detected by a loop antenna. Both antennas rotate in the spin plane and alternately sample field components parallel and perpendicular to the ambient magnetic field. Two dashed lines appear on the spectrogram; the bottom line is the proton cyclotron frequency and the top line is the geometric mean of the electron and proton cyclotron frequencies (both determined from on-board measurements of the magnetic field). The plasma density and the fractional proton composition (discussed later in the section) are high enough such that the geometric mean frequency is close to the lower hybrid frequency.

As can be seen in Figure 1 intense emissions are observed between the lower hybrid frequency and the proton cyclotron frequency. These emissions are centered about the magnetic equator (~0151 UT). Note from the coordinates at the bottom of the plot that the spacecraft passes north to south through the magnetic equator. The lower edge of the emissions is observed to decrease in frequency from 0126 UT to 0151 UT, and rise in frequency from 0151 UT to 0226 UT creating a funnel-shaped image on the spectrogram. The magnetic local time for this observation is about 11 hours, and the geocentric radial distance is near 4 R_E when DE 1 crosses the equator.

Near the equator, this radiation extends up to the lower hybrid frequency ~289 Hz and down to proton cyclotron frequency at 6.9 Hz. The spectrum of the electric field spectral density near the equator crossing (~0151 UT) is shown in Figure 2*a*. The locations of the proton cyclotron frequency f_{cp} and lower hybrid frequency f_{lhr} are indicated by vertical lines. Between 50 Hz and 200 Hz the spectral profile is relatively flat with wave intensities around $\sim 10^{-4}$ V/m$\sqrt{\text{Hz}}$. The wave intensities decrease by 1 order of magnitude near the proton cyclotron frequency and also near the lower hybrid frequency. The electric field intensity peaks when the dipole antenna is perpendicular to the ambient magnetic field, thereby showing that the wave electric field is oriented nearly perpendicular to the magnetic field.

The equatorial plasma waves are also detected by the magnetic loop antenna. The magnetic field is aligned nearly

[1]NASA Marshall Space Flight Center, Huntsville, Alabama.
[2]National Research Council Associate.
[3]University of Iowa, Department of Physics and Astronomy, Iowa City.
[4]Lockheed, Palo Alto, California.
[5]NASA Goddard Space Flight Center, Greenbelt, Maryland.

Paper number 92JA00827.
0148-0227/92/92JA-00827$05.00.

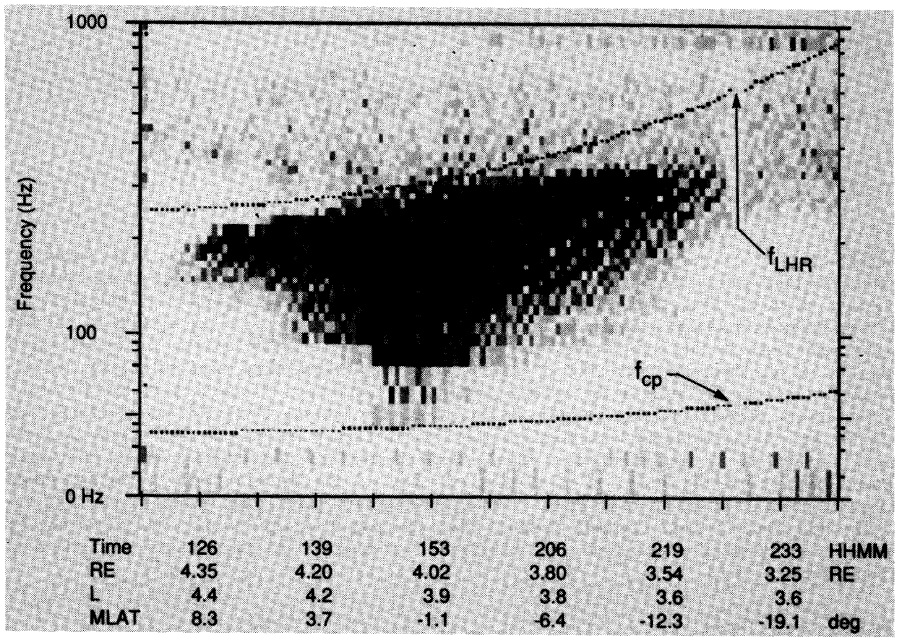

Fig. 1. A spectrogram of electric field spectral density is plotted, which shows a funnel-shaped radiation pattern between the lower hybrid frequency (top dashed curve) and the proton cyclotron frequency (bottom dashed curve). The spectrogram was measured with the plasma wave instrument on the Dynamics Explorer 1 spacecraft at a magnetic local time of 11 hours.

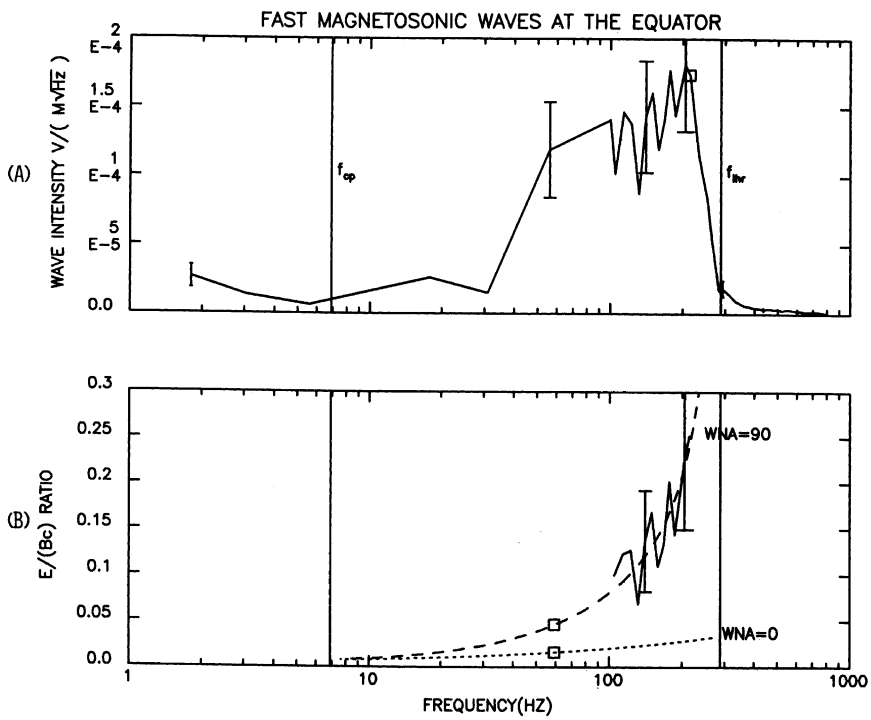

Fig. 2. (*a*) The electric field spectrum measured by the plasma wave instrument at the equator ~0151 UT is plotted. The vertical lines are located at the proton cyclotron frequency f_{cp} = 6.9 Hz, and lower hybrid frequency f_{lhr} = 289 Hz as indicated; (*b*) The ratio of the electric field to the magnetic field, measured by the sweep frequency receiver, is plotted. The two dashed curves are the ratios of the total electric field to magnetic field derived from cold plasma theory for wave normal angles of 0° and 90° as indicated. The good agreement between the measured ratios and the theoretical curve at 90° implies that these waves belong to the fast magnetosonic mode.

parallel to the ambient magnetic field direction. Therefore the wave vector is oriented nearly perpendicular to the ambient magnetic field. In cold plasma theory only one wave mode exits between the lower hybrid frequency and proton cyclotron frequency. This mode is called the whistler mode, and also sometimes in the MHD literature, the fast magnetosonic mode. This mode extends across the proton cyclotron frequency with no cutoffs or resonances (see CMA diagram of *Stix* [1962]).

The ratio of the electric field intensity to that of the magnetic field intensity *E/Bc* is also a good indicator that the waves are fast magnetosonic. The measured *E/Bc* ratio, for the frequency range of 100 Hz to 200 Hz, is plotted in Figure 2*b* along with theoretical curves (dashed) for comparison. The measured *E/Bc* ratio above 200 Hz is not plotted because the magnetic signal drops to the noise level. The theoretical curves are derived from cold plasma theory for wave normal angles $\psi \equiv \tan^{-1}(k_{\parallel}/k_{\perp})$ of 0° and 90° as labeled. The observed *E/Bc* ratios are in good agreement with the theoretical *E/Bc* ratios at wave normal angles near 90° which is consistent with the polarization measurements.

A proton ring distribution in velocity space is detected (see Figure 3) by the energetic ion composition spectrometer (EICS) [*Shelley et al.*, 1981] in the same region where the equatorial wave emissions are observed. The phase space densities are determined by averaging the EICS data over a 10-min interval centered about the magnetic equator. The region of positive slope of the ring distribution is indicated between the contours labeled 3.5 (which is the log of the phase space density given in units of s^3/km^6) and 3.0 by the lightly shaded region. The variability of the 3.0 contour is due to the low counting statistics. Proton ring distributions with much better statistics and smoother contours are commonly detected by the EICS instrument but the quality of the wave data is the major factor in choosing this event for analysis. The proton ring distribution is near the detection limit of 17 keV/el of the EICS instrument and is detected only in the three highest energy channels. The region of the ring distribution that has negative slope occurs at energies greater than the detection limit of the EICS instrument. For this event the proton ring comprises ~1% of the total ion density.

The ring distribution can be pictured as a shell distribution in velocity space with loss cones. The loss cones give the distribution a ringlike or donutlike appearance in velocity space. Using the 3.0 contour, a rough estimate of the loss cone angle of 40° can be made for this event. Therefore most of the protons comprising the ring are mirrored back toward the equator within a magnetic latitude range of ~±26°. For this wave emission, the Alfvén velocity, ~1560 km/s, is located within the region of velocity space occupied by the ring distribution. The location of the Alfvén velocity is indicated (Figure 3) by the darker shaded circular band; the thickness of the band is due to the uncertainty in the fractional compositions of the heavier ions. Since the phase velocity of the fast magnetosonic mode is close to the Alfvén velocity, the ring distributions must strongly interact with these waves. Near geosynchronous orbit, ring distributions associated with

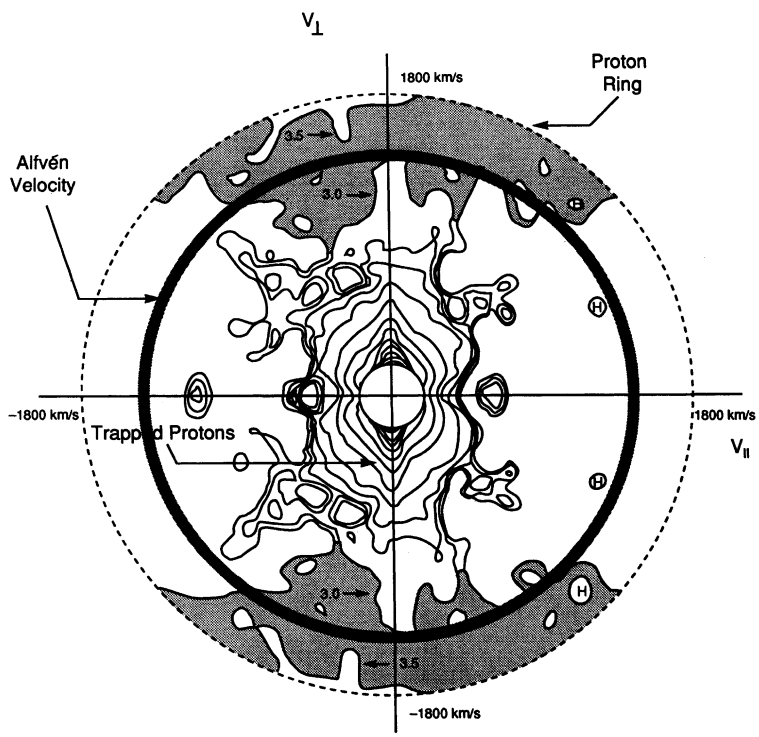

Fig. 3. The velocity space density for protons, measured by the EICS instrument, is plotted. The region of positive slope of the ring distribution is indicated by the shaded region between the contours labeled 3.0 and 3.5. The thick ring of darker shading indicates the location of the Alfvén velocity. The good correspondence between the region of positive slope and the Alfvén velocity implies that the ring is an ideal candidate for the wave source.

low-frequency waves that occur near the proton cyclotron frequency have also been reported and analyzed by *Perraut et al.* [1982] using observations by GEOS 1 and 2.

Ion ring distributions can form as a result of the loss of low-energy ions, thereby causing a "hole" to form in velocity space. These "holes" were first observed by *McIlwain* [1972] and were attributed to the Earthward convection of plasma sheet ions after substorms. The direction in which the plasma sheet ions travel around the Earth depends on the difference between the eastward $\mathbf{E} \times \mathbf{B}/B^2$ drift and the westward $\mu\mathbf{B} \times \nabla B/B^2$ drift. It is believed that the eastward drifting lower-energy ions are lost or arrive later because of differences in the time of flight of the ions convecting in opposite directions around the Earth; therefore, a hole in velocity space develops. An example of how the "holes" form is illustrated in Figure 14 of *Lennartsson et al.* [1981].

A demarcation energy (~EB/∇B) exists where ions with greater energy drift westward and ions with lower energy drift eastward. Near and inside the plasmasphere this demarcation energy is approximately inversely proportional to L shell. *Lennartsson et al.* [1979] showed with observational data that the location of the edge of the hole increases in energy as L shell decreases. This increase in energy with decreasing L shell is also observed with the EICS instrument. During this event the ring distribution moves up and out of the energy/charge range of EICS at a L shell below ~3.9 R_E.

The plasma density, calculated from the upper hybrid frequency, is observed to rise from ~10 cm^{-3} at 0126 UT to ~40 cm^{-3} at 0151 UT, where the density peaked briefly before rising again as DE 1 enters the plasmasphere. The bulk of the ion density is composed of low-energy thermal protons ~1 — 10 eV flowing along the magnetic field lines, and of equatorially trapped protons (indicated in Figure 3) ~50 eV. Near the equator the trapped protons are estimated to make up about 75% of the ion plasma population. The protons are estimated, from the retarding ion mass spectrometer, to make up about 99% of the cold (<50 eV) plasma ion population.

To summarize the observations funnel-shaped, fast magnetosonic waves centered about the magnetic equator are observed along with low-energy field-aligned flow and equatorially trapped protons which comprise the bulk of the ion density. The proton ring distribution comprises about 1% of the ion density and the ring velocity is close to the Alfvén velocity. In the next section a qualitative explanation of the funnel-shaped structure is given in terms of cold plasma wave propagation and growth and damping of the waves.

3. INTERPRETATION

A qualitative explanation of the funnel-shaped equatorial emissions is given in this section. First ray-tracing calculations in a cold plasma are used to investigate the wave propagation, and then a linear growth analysis is used to identify where strong growth or damping occurs.

3.1 *Wave Propagation*

Cold plasma ray-tracing calculations can be used to follow the spatial propagation of the waves because the bulk thermal ion velocity ~70 km/s is much smaller than the Alfvén velocity V_A ~1560 km/s. The code used was developed by *Green et al.* [1977] and is an extension to three dimensions of the two-dimensional (2-D) code written by *Shawhan* [1966]. The Earth's magnetic field is modeled by a dipole.

The density model used in this study consists of trapped and constant background components. The trapped component varies linearly in L shell with a latitudinal profile that maximizes at the equator. The density model parameters are chosen such that the modeled densities are in good agreement (within >25%) with the measured densities which are based on observations of upper hybrid resonance emission. The density model, although 2-D, is based on a 1-D slice through the equatorial region with varying L shell and latitude. Although the model is consistent with the observed density profile, it is not a unique representation of equatorial densities. The sensitivity of the ray-tracing results to variations in the model was tested by allowing a 25% variation in the slope of the L shell profile and in the extent of the latitudinal trapping. Neither variation produced significant change in the results that are presented here. First a brief discussion of resonances near harmonics of the ion cyclotron frequency is given.

As the waves propagate through space, they encounter resonances whenever the wave frequency is near a harmonic of the proton cyclotron frequency. At resonances the WKB approximation breaks down and either mode conversion, tunneling, reflection, or resonant absorption of the wave energy occurs. *Ngan and Swanson* [1977] estimated the tunneling coefficient at harmonics of the ion cyclotron frequency, when the wave vector is perpendicular to the ambient magnetic field. Their tunneling coefficient for the second harmonic is

$$\eta^2 = \frac{\pi \omega_{pi} R_0 \beta_i}{c},$$

where $\beta_i \sim 10^{-3}$ is the thermal ion velocity squared divided by the Alfvén velocity squared, ω_{pi} is the ion plasma frequency, c is the speed of light, and R_0 is the spatial scale length. The tunneling coefficients for higher harmonics are given approximately by $\eta_n \sim \eta_2(10\beta_i)^{n-2}$. At the equator $R_0 \sim |B/\nabla B| = r/3$. The tunneling coefficient is very small $\eta_2 \sim 0.2$, and therefore the transmission coefficient $e^{-\eta_n}$ is very close to 1.

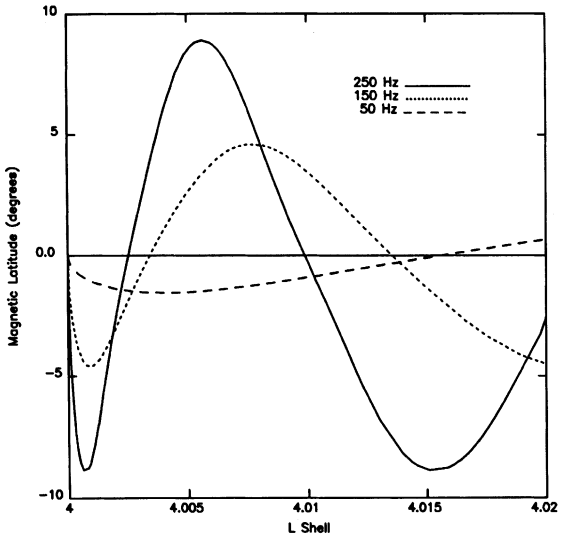

Fig. 4. Ray paths for frequencies of 50, 150, and 250 Hz are plotted as a function of invariant latitude and L shell. These paths illustrate the confinement of these waves to the magnetic equator.

Since the transmission coefficient maps the wave energy from the magnetosonic mode WKB solution on one side of the resonance to the magnetosonic mode WKB solution on the other, ray-tracing calculations can still be used to follow the ray path.

To illustrate the how fast magnetosonic waves propagate through space examples of ray paths for different frequencies are shown in Figure 4. The waves are launched in the meridian plane, on the equator at L=4, each with an initial wave normal angle, close to 90° (Figure 2*b*), of 88°. The perpendicular components of the group velocities are initially in the azimuthal direction. The ray-tracing calculations indicate that the rays are refracted back and forth across the equator as they propagate. At the turning point the wave normal angle ψ is perpendicular

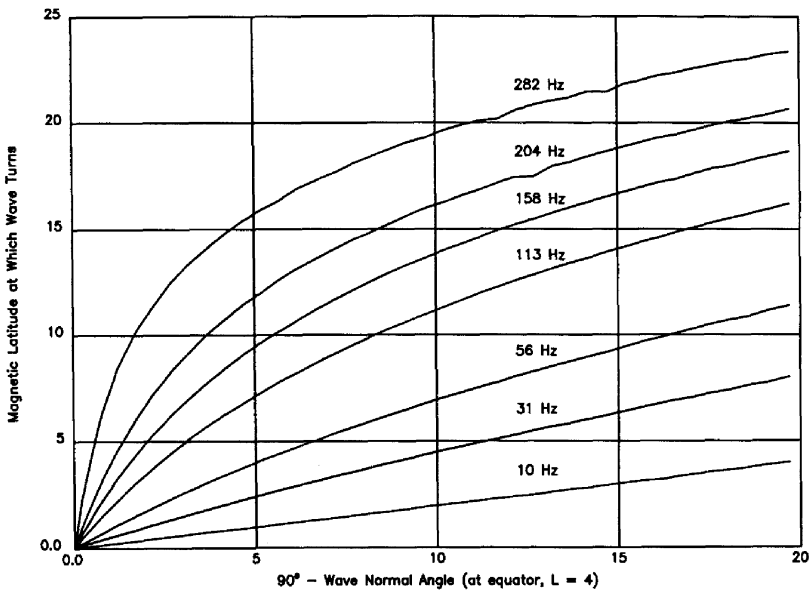

Fig. 5. The relationship between the magnetic latitude at which the waves are refracted back toward the equator (y axis) and the equatorial deviation of the wave normal angle from 90° (at L = 4) are plotted for different frequencies. This plot shows that the lower-frequency waves are more strongly confined to the equator than the higher-frequency waves.

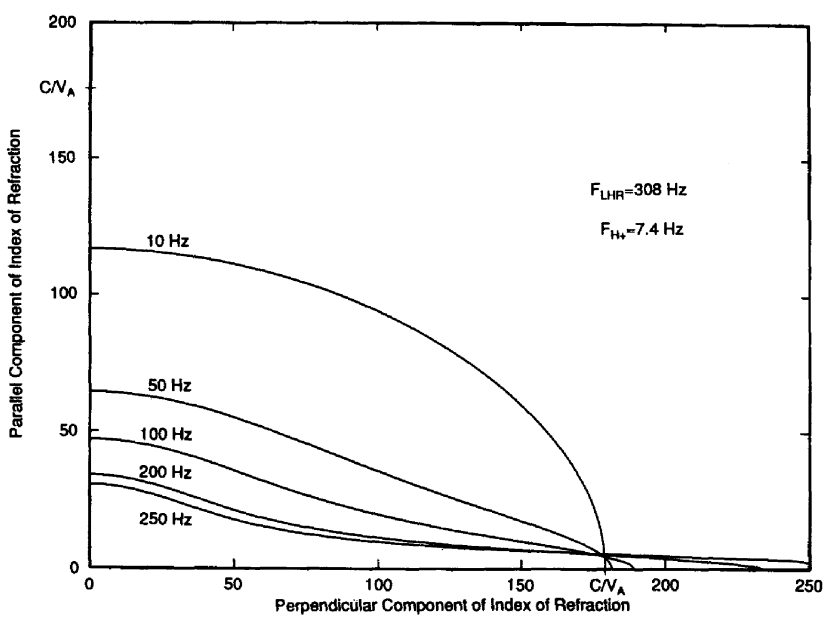

Fig. 6. Index of refraction surfaces are plotted for different frequencies based on observations at L = 4.

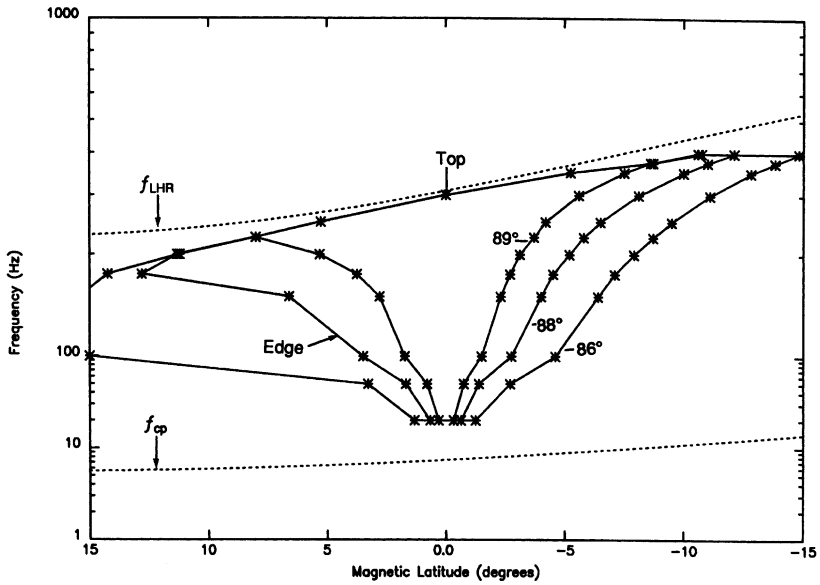

Fig. 8. Reproduction of the funnel from ray-tracing calculations. The funnel outlines are produced by waves with equatorial wave normal angles of 89°, 88°, and 86° as labeled. The funnel outline for 88° is close to the outline of observed emissions in Figure 1.

inner edge of the ring, where $\partial F/\partial v_\perp > 0$, growth should occur, and when $(v_{\parallel, RES}, v_{phase, \perp})$ lies on the outer edge of the ring, where $\partial F/\partial v_\perp < 0$, damping should occur.

The hot plasma code WHAMP [*Rönnmark*, 1982] is used to solve the dispersion relation. The general form of the distribution function used by WHAMP is shown in the theory section of *André et al.* [1986]. The ring distribution is approximated in WHAMP by subtracting a cooler bi-Maxwellian from a warmer bi-Maxwellian. The parameters used in WHAMP are listed in Table 1. The parameters are defined as follows: $A = T_\perp/T_\parallel$ for the added bi-Maxwellian, $B = T_\perp/T_\parallel$ for the subtracted bi-Maxwellian, and Δ is a relative weighting between the added and subtracted bi-Maxwellian terms. The ring parameters are chosen such that the phase space density of the ring maximizes at a velocity slightly larger than the Alfvén velocity. The values of the real part of the dispersion relation given by WHAMP are found to be within 2% to 5% of the values predicated by the cold plasma approximation. Results are presented for bulk electron temperatures of 1 eV; however, calculations were done for electron temperatures up to 500 eV without significant changes in the growth rates.

For wave normal angles very close to 90° the growth rates are sharply peaked around $n f_{cp}$ because the parallel resonance velocity changes rapidly with frequency due to the smallness of $k_\parallel$, so f has to be close to $n f_{cp}$ in order for a sufficient number of protons to resonate with the waves. As $k_\parallel$ increases the resonance condition is easier to satisfy and the spread in unstable frequencies $\delta f > \| f - n f_{cp} \|$ increases, while the maximum in growth rate decreases. This decrease is due to the increase in phase velocity as the wave normal angle decreases (Figure 6) causing $\partial F/\partial v_\perp$ $|(v_\perp = v_{phase,\perp})$ to become smaller. Finally, the wave normal angle increases to a point where $(v_{\parallel, RES}, v_{phase, \perp})$ lies on the outer edge of the ring and damping occurs. Similar growth/damping rates were also obtained by approximating the ring distribution by subtracting a colder Maxwellian from a hotter one (shell distribution), with some differences occurring because of the lack of a loss cone.

The spatial growth rates of the waves are plotted in Figure 9 for magnetic latitudes of 0°, 4°, and 8° along $L = 4$. The wave normal angle of 89.95°, used in the growth rate calculations, was chosen to be close to 90°, which is the wave normal angle at which the waves refract back toward the equator. The parameters specifying the ring distribution are held constant because the spatial extent of the ring distribution of ~±26° magnetic latitude, as discussed in section 2, is much larger than the magnetic latitudes for which the growth rate calculations are made. The growth rates are close to the largest values that can be obtained from WHAMP for the fast magnetosonic mode and given plasma parameters.

The growth rate peaks at harmonics of the local proton cyclotron frequency and is narrow-banded because the wave normal angle is very close to 90°. Between the positive harmonics the growth rate drops to zero, except for extremely narrow band regions (not shown) on either side of the positive peaks where damping occurs. Comparison of the frequency range for which spatial growth occurs indicates that the region of positive growth becomes restricted to higher frequencies at larger magnetic latitudes, as shown in Figure 9. This trend occurs because the Alfvén velocity increases with magnetic latitude and only the higher-frequency wave components, which have phase velocities smaller than the Alfvén velocity, can still

TABLE 1. Parameters Used in WHAMP

Species	n, cm^{-3}	$T_\parallel$, keV	A	B	Δ
H+	39.6	0.001	1.0	-	1.0
H+	0.4	23.4	1.25	1.136	0.0
e-	40.0	0.001	1.0	-	1.0

Magnetic field strength = 486γ.

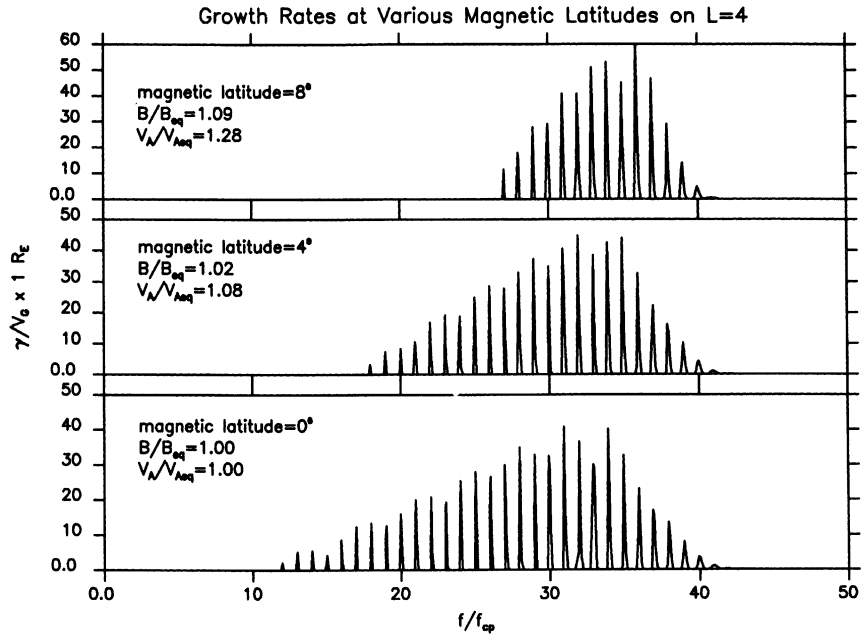

Fig. 9. The spatial growth rates at magnetic latitudes of $L = 0°$, 4°, and 8° are plotted along $L = 4$. In the computations the ring parameters are held constant, and the wave normal angle is 89.95°.

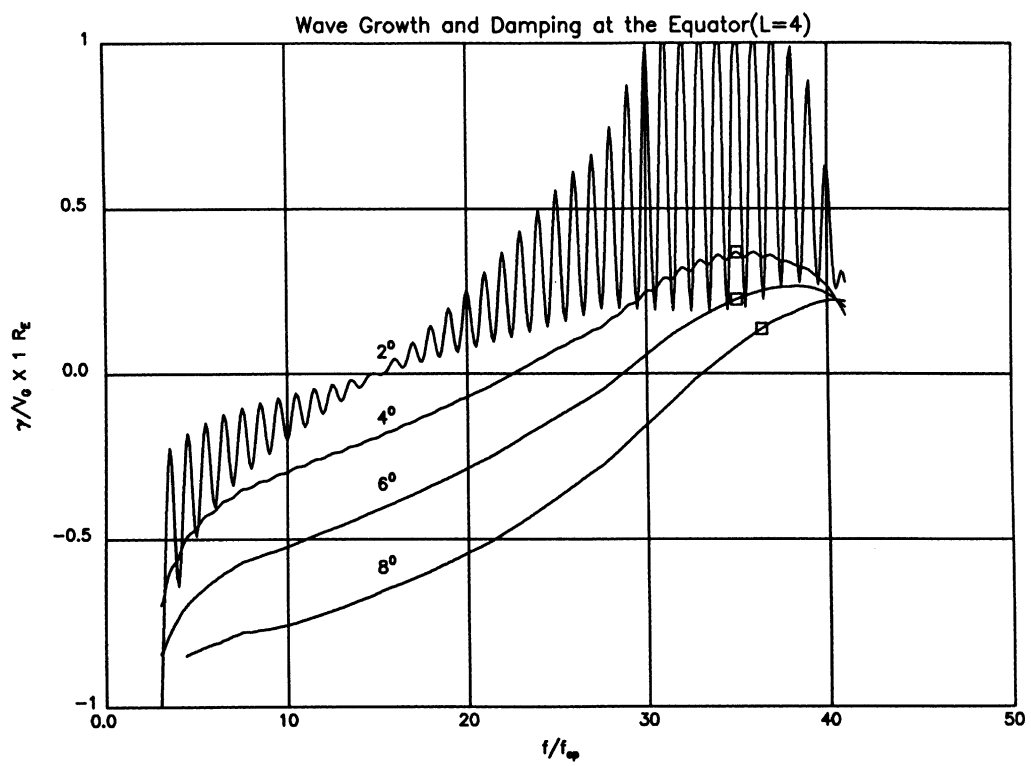

Fig. 10. The spatial growth/damping rate times 1 R_E, at the equator, $L = 4$, is plotted against the frequency normalized by the proton cyclotron frequency f_{cp}. Each curve corresponds to a different magnetic latitude, as labeled, at which the waves are refracted back toward the equator.

interact with the region of positive slope in the ring distribution.

To illustrate wave damping at the equator at L=4, the spatial growth/damping rate of waves with different frequencies is computed using WHAMP and is shown in Figure 10. The y axis is the spatial growth/damping rate times 1 R_E, and the x axis is the wave frequency divided by the proton cyclotron frequency at the equator. Each curve is labeled by the magnetic latitude at which the waves are refracted back toward the equator. The equatorial wave numbers used in WHAMP are determined from interpolation of the curves shown in Figure 5. For each curve in Figure 10 the wave normal angle increases toward 90° as the frequency increases. The increase in wave normal angle with frequency is very apparent in the 2° curve where the resonant overlap of neighboring harmonics is reduced as the wave normal angle increases. This dependence leads to sharper peaks in the growth rate at higher frequencies. Usually the damping is broad-banded. Figure 10 shows that low-frequency waves experience stronger damping than high-frequency waves.

The following conclusions are drawn from linear growth/damping rate analysis: (1) Maximum growth occurs at wave normal angles within 0.2° of 90° and at frequencies very close to $n f_{cp}$. (2) Damping occurs at all frequencies when the wave normal angle deviates more than a few degrees away from 90°, which corresponds to increasing $k_{\parallel}$. Therefore, if the wave frequency is close to a harmonic of the proton cyclotron frequency, the spatial growth of the waves is strongest at the turning points and the wave damping maximizes around the equator. The damping, when it occurs, occurs over a broad range of frequencies. Wave growth off the equator and wave damping in the equatorial region indicate that equatorial wave normal angle distributions which lead to funnels are likely to occur.

4. DISCUSSION

The analysis presented above indicates that the primary factor in explaining the funnel is wave propagation. Ray-tracing calculations show that for a broad range of wave normal angles, waves lower in frequency are more closely confined to the magnetic equator than waves higher in frequency. Predicting how the intensity of the radiation varies with magnetic latitude requires a more detailed analysis involving ray path integrated gains. The region in which largest wave growth occurs corresponds to the point at which the waves are refracted back toward the equator, and then only if the wave frequency is close to a harmonic of the local proton cyclotron frequency. As the wave starts to propagate toward the equator the growth rate decreases due to the decreasing wave normal angle and the changing proton cyclotron frequency. A point is reached along the ray path where the wave then starts to damp as it propagates toward the equator. Damping of the waves by the proton ring distribution is largest in the vicinity of the equator. As the wave propagates back and forth across the equator the likelihood of the wave remaining in resonance with a proton cyclotron harmonic at the refraction point is small so additional growth becomes less likely and only damping occurs.

One problem in doing path-integrated gains involves choosing an adequate model of how the ring density, velocity, temperature, and loss cone angle vary with L shell and magnetic local time. Also, the proton ring distributions strongly interact with the waves, leading to quasi-linear diffusion which path-integrated gains cannot take into account. Because the waves can possibly cause the ring ions to diffuse across the demarcation energy where the convection direction reverses, a complicated interplay between convection and velocity space diffusion could occur. The ring distribution is probably a combination of a flattened distribution due to quasi-linear diffusion and a free energy source due to fresh ring protons convecting into the region. The extent to which the plateau forms is probably dependent upon the time it takes the protons to convect through the region in which the waves exist.

Another problem in calculating ray path integrated gains is that the strongest wave growth occurs near harmonics of the proton cyclotron frequency. The use of the WKB approximation is more suspect near resonances. Also, the group velocity changes rapidly with wave normal angle for wave normal angles close to 90°, and this has to be folded into the path-integrated gain calculations.

One final comment is that the equatorial wave emissions do not always have a funnellike appearance. We believe that part of the explanation is due to the changing inclination of the DE 1 orbit with equatorial plane. Most of the funnel examples occur when DE 1 is near apogee, when it is sampling narrow range of L shells around the equator, and no funnel observations have been obtained when DE 1 is crossing the equator at altitudes below 2 R_E when it is sampling a wider range in L shell.

In conclusion, the funnel-shaped structure is largely a wave propagation effect in which lower-frequency waves are more strongly confined to the magnetic equator, than that of higher-frequency waves. Wave growth and damping calculations are also consistent with funnel-shaped radiation patterns. Wave damping is stronger at the lower frequencies in the vicinity of the equator and wave growth becomes more restricted to higher frequencies at larger magnetic latitudes. It is clear that more detailed path-integrated gain calculations and plasma simulations of the interaction of fast magnetosonic waves with energetic equatorial ion distributions are justified. Such calculations would allow us to understand more fully the exchange of energy between ions and waves.

Acknowledgments. We gratefully acknowledge K. Rönnmark and M. André for the source code and documentation to WHAMP. We would like to thank B. Ledley for the magnetonmeter data. The work at Marshall Space Flight Center was supported by the Dynamics Explorer Program, UPN 370-13-19. The work at Iowa was supported by NASA under grant NAG5-310. The work at Lockheed was supported by NASA under contract NAS5-33032. This work was done while S. A. Boardsen, an NRC post doctorate, held a National Research Council-Marshall Space Flight Center Research Associateship.

The Editor thanks I. Roth and M. A. Temerin for their assistance in evaluating this paper.

REFERENCES

André, M., M. Temerin, and D. Gorney, Resonant generation of ion waves on auroral field lines by positive slopes in ion velocity space, *J. Geophys. Res.*, *91*, 3145, 1986.

Curtis, S. A., Equatorial trapped plasmasphere ion distributions and transverse stochastic acceleration, *J. Geophys. Res.*, *90*, 1765, 1985.

Green, J. L., D. A. Gurnett, and S. D. Shawhan, The angular distribution of auroral kilometric radiation, *J. Geophys. Res.*, *82*, 1825, 1977.

Gurnett, D. A., Plasma wave interactions with energetic ions near the magnetic equator, *J. Geophys. Res.*, *81*, 2765, 1976.

Lennartsson, W., E. G. Shelley, R. D. Sharp, and R. G. Johnson, Some initial ISEE-1 results or the ring current composition and dynamics during the magnetic storm of December 11, 1977, *Geophys. Res. Lett.*, *6*(6), 483, 1979.

Lennartsson, W., R. D. Sharp, E. G. Shelley, R. G. Johnson, and H. Balsiger, Ion composition and energy distribution during 10 magnetic storms, *J. Geophys. Res.*, *86*, 4628, 1981.

McIlwain, C. E., Plasma convection in the vicinity of the

geosynchronous orbit, in *Earth Magnetospheric Processes*, edited by B. M. McCormac, p. 268, D. Reidel, Hingham, Mass., 1972.

Ngan, Y. C., and D. G. Swanson, Mode conversion and tunneling in an inhomogeneous plasma, *Phys. Fluids, 20(11)*, 1920, 1977.

Olsen, R. C., S. D. Shawhan, D. L. Gallagher, J. L. Green, C. R. Chappell, and R. R. Anderson, Plasma observations at the Earth's magnetic equator, *J. Geophys. Res., 92*, 2385, 1987.

Perraut, S., A. Roux, P. Robert, R. Gendrin. J. Sauvaud, J. Bosqued, G. Kremser, and A. Korth, A systematic study of ULF waves above F_{H^+} from GEOS 1 and 2 measurements and their relationshiops with proton ring distributions, *J. Geophys. Res., 87*, 6219, 1982.

Rönnmark, K., WHAMP-waves in homogeneous, anisotropic, multicomponent plasmas, *Kiruna Geophys. Inst., Rep. 179*, Kiruna Geophysical Institute, Kiruna, Sweden, 1982.

Russell, C. T., R. E. Holzer, and E. J. Smith, Ogo 3 observations of energetic heavy ions during a geomagnetic storm, *J. Geophys. Res., 75*, 755, 1970.

Schmidt, G., *Physics of High Temperature Plasmas*, Academic, San Diego, Calif., 1979.

Shawhan, S. D., VLF ray tracing in a model ionosphere, *Res. Rep. 66-33*, Dep. of Phys. and Astron., University of Iowa, Iowa City, 1966.

Shawhan, S. D., D. A. Gurnett, and D. L. Odem, The plasma wave and quasistatic electric field instrument (PWI) for Dynamics Explorer-A, *Space Sci. Instrum., 5*, 535, 1981.

Shelley, E. G., D. A. Simpson, T. C. Sanders, E. Hertzberg, H. Balsiger, and A. Shielmetti, The energetic ion composition spectrometer (EICS) for the Dynamics Explorer-A, *Space Sci. Instrum., 5*, 443, 1981.

Stix, T. H., *The Theory of Plasma Waves*, McGraw-Hill, New York, 1962.

S. A. Boardsen and D. L. Gallagher, NASA Marshall Space Flight Center, Huntville, AL 35812.

J. L. Green, NASA Goddard Space Flight Center, Greenbelt, MD, 20771.

D. A. Gurnett, University of Iowa, Department of Physics and Astronomy, Iowa City, IA 52242.

W. K. Peterson, Lockheed Missiles and Space Company, Inc., Space Sciences Laboratory, Palo Alto, CA 94204.

(Received October 4, 1991;
revised February 27, 1992;
accepted March 2, 1992.)